An inhibitor of mTOR reduces neoplasia and normalizes p70/S6 kinase activity in *Pten*$^{+/-}$ mice

Katrina Podsypanina*, Richard T. Lee*, Chris Politis*, Ian Hennessy*, Allison Crane*, Janusz Puc*, Mehran Neshat†, Hong Wang‡, Lin Yang*, Jay Gibbons§, Phil Frost§, Valley Dreisbach¶, John Blenis¶, Zbigniew Gaciong‖, Peter Fisher*, Charles Sawyers†, Lora Hedrick-Ellenson‡, and Ramon Parsons*,**

*Institute of Cancer Genetics, Departments of Pathology and Medicine, College of Physicians and Surgeons, Columbia University, 1150 St. Nicholas Avenue, Russ Berrie Pavilion, New York, NY 10032; †Department of Medicine, Molecular Biology Institute, University of California, Los Angeles, CA 90095-1678; ‡Department of Pathology, Weill Medical College of Cornell University, 1300 York Avenue, New York, NY 10021; §Wyeth-Ayerst Research, 401 Middletown Road, Pearl River, NY 10965; ¶Department of Cell Biology, Harvard Medical School, Boston, MA 02115; and ‖Department of Internal Diseases and Hypertension, Medical University of Warsaw, 1a Banacha Street, 02-097 Warsaw, Poland

Edited by Bert Vogelstein, Johns Hopkins Oncology Center, Baltimore, MD, and approved June 14, 2001 (received for review February 6, 2001)

PTEN phosphatase acts as a tumor suppressor by negatively regulating the phosphoinositide 3-kinase (PI3K) signaling pathway. It is unclear which downstream components of this pathway are necessary for oncogenic transformation. In this report we show that transformed cells of PTEN$^{+/-}$ mice have elevated levels of phosphorylated Akt and activated p70/S6 kinase associated with an increase in proliferation. Pharmacological inactivation of mTOR/RAFT/FRAP reduced neoplastic proliferation, tumor size, and p70/S6 kinase activity, but did not affect the status of Akt. These data suggest that p70/S6K and possibly other targets of mTOR contribute significantly to tumor development and that inhibition of these proteins may be therapeutic for cancer patients with deranged PI3K signaling.

The *PTEN* tumor suppressor is mutated in a wide variety of human sporadic and inherited cancers (1). PTEN acts as a negative regulator of the phosphoinositide 3-kinase (PI3K) signaling pathway by dephosphorylating the second messengers phosphatidylinositol-3,4,5-trisphosphate [PtdIns(3,4,5)P_3] and phosphatidylinositol-3,4-bisphosphate [PtdIns(3,4)P_2] at the D3 position of the inositol ring, thereby opposing PI3K function (2). Consistent with the role of PTEN as a PtdIns(3,4,5)P_3 phosphatase, *Pten*-deficient cells have elevated levels of intracellular PtdIns(3,4,5)P_3 (3, 4).

In flies, expression of PTEN can rescue lethality caused by overexpression of d-PI3K (Dp110) or the fly insulin receptor (*Inr*) (5, 6). The loss-of-function phenotypes of dPTEN, increased cell size and proliferation, are suppressed by inactivating mutations in *dAKT1* and the translational initiation factor *eif4A*, suggesting that dPTEN acts through the AKT-signaling pathway to regulate translation (7). Loss-of-function mutations in another translational regulator, *Drosophila* p70/S6 kinase (*dS6K*) (8), as well as its upstream regulators *dPI3K*, *Inr*, and *chico* (fly insulin receptor substrate 1–4) decrease cell size in *Drosophila* (9). For p70/S6 kinase (S6K) the ability to control cell size is conserved in mammals (10, 11). In addition, *S6K*$^{-/-}$ mouse embryonic stem cells have a defect in proliferation with a greater proportion of cells in G_0/G_1 (10). The increased size and proliferation of dPTEN-deficient cells is consistent with the antagonistic role of PTEN in the PI3K-signaling pathway and suggests that PTEN may play a role in regulating S6K.

Mitogen-induced activation of S6K is mediated through the PI3K-dependent phosphorylation of several residues (12, 13). This activation is in part performed by 3-phosphoinositide-dependent kinase 1 (14, 15). In addition, membrane-tethered AKT is able to activate S6K, whereas untethered, activated mutants of AKT do not have this effect (16). Activation of S6K can be blocked by the pharmacological agent rapamycin (17, 18). Rapamycin has potent immunosuppressant and tumor inhibitory activities (19). To exert its effect, rapamycin binds an immunophilin, FK-506-binding protein 12, and this complex inhibits the cellular target of rapamycin, mTOR/RAFT/FRAP (20–22). mTOR is a member of the ataxia-telangiectasia-mutated (ATM) family of kinases that seems to function in a checkpoint for nutritional status in G_1 and in response to the PI3K/AKT pathway (23, 24). AKT can directly phosphorylate mTOR (25, 26), although the impact of this phosphorylation on the activity of mTOR has not been firmly established. Several studies have demonstrated control of S6K activity by mTOR by direct (27, 28) and indirect (29–31) mechanisms. Recent studies of the fly homolog of mTOR, dTOR, have demonstrated that mutants of dTOR have reduced cell size and proliferation and fail to develop to maturity (32, 33). Overexpression of dS6K rescued dTOR mutants from embryonic lethality (32). Moreover, the large cell size and hyperproliferative phenotypes of dPTEN were completely masked by mutation of dTOR. These data suggest that dS6K is a critical downstream target of dTOR and dPTEN.

S6K is amplified and overexpressed in breast cancer, which suggests a potential oncogenic function (34, 35). Constitutive activation of S6K in PTEN-deficient tumor cells has been reported previously and can be corrected by reintroduction of PTEN (36). To investigate the potential contribution of the mTOR/S6K pathway to the transformation induced by *Pten* loss, we examined the effect of inhibiting mTOR with the rapamycin ester CCI-779 in the *Pten*$^{+/-}$ mouse tumor model system.

Materials and Methods

Mice and Treatment. *Pten*$^{+/-}$ mice were generated as described (37). The rapamycin analog CCI-779 was provided by Wyeth Ayerst Laboratories (Marietta, PA). The drug was first diluted to 50 mg/ml in 100% ethanol and then quickly mixed with 5% Tween-80 (GIBCO/BRL)/5% polyethylene glycol-400 (Sigma) to a 2 mg/ml drug/4% ethanol final concentration. The drug solution, or the vehicle alone, was delivered to mice through the tail vein at a dose of 20 mg/kg (10 μl/g of body weight).

Histology. Mice were given i.p. injections of 125 mg/kg of BrdUrd (Sigma) 1 h before euthanasia. Organs for histological analysis

This paper was submitted directly (Track II) to the PNAS office.

Abbreviations: PI3K, phosphoinositide 3-kinase; CAH, complex atypical hyperplasia; PtdIns(3,4,5)P_3, phosphatidylinositol-3,4,5-trisphosphate; TUNEL, terminal deoxynucleotidyltransferase-mediated dUTP nick end labeling.

See commentary on page 10031.

**To whom reprint requests should be addressed. E-mail: rep15@columbia.edu.

The publication costs of this article were defrayed in part by page charge payment. This article must therefore be hereby marked "*advertisement*" in accordance with 18 U.S.C. §1734 solely to indicate this fact.

were kept in 10% formalin overnight, then changed to 70% ethanol. Paraffin embedding was performed no later than a week after organ collection. For the long-term CCI-779 experiment, paraffin tissue blocks from individual mice were coded from 1 to 20 and hematoxylin/eosin stains of those were analyzed in blinded fashion by at least three investigators (K.P., R.P., P.F., and L.H.-E.). Catecholamines were measured from blood collected at the time of death with an HPLC kit from Bio-Rad according to the manufacturer's instructions.

Immunohistochemistry. All immunohistochemistry stains were performed on 4-μm-thick tissue slices as described (38). The following antibodies and dilutions were used: mouse monoclonal anti-BrdUrd (Becton Dickinson) 1:200, rabbit polyclonal anti-PTEN (Neomarkers Ab-2) 1:500, rabbit polyclonal anti-phospho-AKT (Ser-473; NEB, Beverly, MA) 1:50, and mouse monoclonal anti-p27 (Transduction Laboratories, Lexington, KY) 1:500. Apoptosis was measured with the terminal deoxynucleotidyltransferase-mediated dUTP nick end labeling (TUNEL) assay. Positive controls included irradiated organs and DNase-treated sections. The apoptotic index was calculated similar to the BrdUrd incorporation index (see below). TUNEL staining was performed on paraffin-embedded sections that were deparaffinized in xylenes and transferred to 95% methanol and then water. Slides then were treated with 20 μg/ml proteinase K for 20 min, washed, and endogenous peroxidases were blocked in 3% H_2O_2 in methanol, dipped in terminal deoxynucleotidyltransferase (TdT) buffer, and incubated for 60 min at 37°C with the TdT/Bio-16-dUTP mix. After a wash, slides were incubated with Avidin-horseradish peroxidase (Dako) 1:400 for 20 min. The horseradish peroxidase substrate 3-amino-9-ethylcarbazole was incubated with the slides in a glass contained in the acetate buffer (10.5 mM acetic acid/80 mM Na acetate solution, pH 5.5) until full color development and counterstained with Mayer's hematoxylin.

Measurement of Proliferation, Apoptosis, Lesion Size. Anti-BrdUrd and TUNEL-stained uterine cross-sections (3–5 per mouse) and adrenal medullas were acquired at ×40 magnification by a Diagnostic Instruments (Sterling Heights, MI) digital SPOT (Diagnostic Instruments, Sterling Heights, MI) camera in Adobe PHOTOSHOP. Vertical and horizontal diameters of the uteri, complex atypical hyperplasia (CAH) lesions, and medullas were measured by using the loop tool. All BrdUrd- and TUNEL-positive cells were counted in the secretory epithelium of the uterus and in the medulla. Resulting numbers were entered in a Microsoft EXCEL spreadsheet. Areas were calculated by averaging horizontal and vertical diameters to obtain the radius. The BrdUrd and TUNEL indexes for adrenals in all experiments and untreated and short-term-treated uterine samples were calculated by dividing the absolute number of positive cells by the uterine or adrenal section area. In transition zones, up to 100 nuclei were counted in transformed and nontransformed regions, and the BrdUrd index was calculated per total number of nuclei. For the long-term treatment group, all secretory epithelial cells were counted in one section per mouse, and the BrdUrd and TUNEL index was calculated per total number of cells. Lesions in stained sections were acquired at ×25 magnification and measured with use of NIH IMAGE 1.62. *P* values were calculated with Student's *t* test. Error bars represent standard deviation. *P* values were obtained by comparing two given groups by Student's two-tailed *t* test.

Western Blotting. Frozen uteri and adrenals were ground in liquid nitrogen by mortar and pestle and tissue powder was transferred into 1× loading buffer and boiled for 5 min. Samples were spun and soluble protein concentrations were determined before loading on a gel. Antibodies to AKT and phospho-389-S6K were obtained from NEB and anti-tubulin was purchased from Babco (Richmond, CA). The C-2 antibody for S6K was used.

***Pten* Loss of Heterozygosity.** To study loss of heterozygosity of *Pten* in the CAH of the endometrium, the wild-type and mutant alleles were amplified from DNA prepared from microdissected, formalin-fixed, paraffin-embedded uterine lesions. Both the mutant and wild-type alleles were amplified simultaneously by using a common 5′ primer within intron 4 and two 3′ primers, one within exon 5 of *Pten* and one within the *Pgk* gene: GGGATTATCTTTTTGCAACAGT (Pten 5′), GGCCTCTTGTGCCTTTA (Pten 3′), and TTCCTGAC-TAGGGGAGGAGT (Pgk 3′). Tail DNAs of a healthy PTEN heterozygous mouse and a wild-type mouse were used as controls. PCR was performed in 50-μl reactions containing 10 mM Tris·HCl (pH 9.2), 1.5 mM $MgCl_2$, 75 mM KCl, 0.4 μM of each 3′ primer, 0.8 μM 5′ primer, 160 μM each dNTP, and 2.5 units of *Taq* polymerase(GIBCO). Forty cycles of PCR were performed; each cycle consisted of 1 min at 95°C, 1 min at 57°C, and 1 min at 72°C followed by a single 5-min extension at 72°C. To study the loss of heterozygosity of *Pten* in the adrenals, Southern blotting was performed on DNA extracted from normal adrenals, pheochromocytomas, and tail DNA as a control. 3′ probe flanking the targeted region was used on the *Pst*I-digested DNA.

S6K Assay. The S6K kinase assay was performed essentially as described previously (10, 39). In short, frozen uteri of 35- to 50-week-old animals were homogenized in 10 mM KPO_4, 10 mM $MgCl_2$, 1 mM EDTA, and 0.1% Nonidet P-40 in the presence of protease and phosphatase inhibitors. Protein concentration was measured from the soluble fraction, and samples were normalized to equal protein concentration in each experiment. S6K was immunoprecipitated from tissue lysates with protein A/G agarose (C-18, Santa Cruz Biotechnology) at 4°C overnight. Samples were washed twice in the lysis buffer followed by a wash in kinase buffer (20 mM Tris, pH 7.5/10 mM $MgCl_2$/0.1 mg/ml BSA/0.4 mM DTT). The kinase reaction was performed at 30°C for15 min in the presence of 100 μM ATP, 200 μCi/ml [γ-^{32}P]ATP, and 125 μM S6 peptide substrate (Upstate Biotechnology, Lake Placid, NY). Stopped reactions were loaded onto phosphocellulose columns (Pierce) and unbound label was washed with 75 mM phosphoric acid. Bound, labeled probe was measured in a liquid scintillation counter.

Results

To use the *Pten*$^{+/-}$ mice for preclinical trials of candidate drugs, the penetrance and variability of tumor phenotypes was documented. Multifocal CAH developed in the uterine secretory epithelium of almost every (29/30) *Pten*$^{+/-}$ female mouse by 26 weeks of age. Two types of transformed lesions were present: cribriform glands and transformed cysts. Cribriform glands were defined as continuous foci of crowded glands. Transformed cysts were defined as cavities fully or partially lined with transformed epithelium. Some cavities appeared empty and some were filled with necrotic masses. In some sections a stretch of normal epithelium was observed in the cyst wall, with a clear transition zone between normal and transformed epithelium. Some of the older wild-type mice had cysts in the endometrium, but the epithelial lining was never transformed. We also observed that nearly all of the *Pten*$^{+/-}$ mice developed neoplasia of the chromaffin cells of the adrenal medulla by 6 months (48/49; Fig. 1 *A* and *B*). This neoplasia was bilateral and multifocal. In mice more than 1 year of age the tumors were frequently diagnosed as pheochromocytomas. Elevated serum levels of both norepinephrine ($P = 0.069$) and epinephrine ($P = 0.039$) suggested that the tumor cells retained some of the functional characteristics of the chromaffin cell (Fig. 1 *C* and *D*).

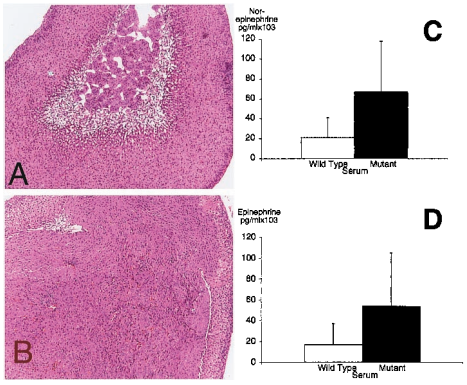

Fig. 1. *Pten*$^{+/-}$ mice develop pheochromocytomas of the adrenal medulla. Morphology of the wild-type adrenal (*A*) and the *Pten*$^{+/-}$ adrenal containing a pheochromocytoma (*B*). (Magnification, ×40.) The normal medulla can be seen in the center of the wild-type adrenal cortex. Paraffin sections were stained with hematoxylin/eosin. PTEN$^{+/-}$ animals (mutant) have elevated levels of serum norepinephrine (*C*) and epinephrine (*D*) relative to wild type.

Proliferation Is Increased in the Lesions. Loss of *Pten* has been linked to both increased proliferation and to defects in apoptosis. To investigate whether either of these mechanisms contributed to uterine neoplasia, we first studied the frequency of BrdUrd incorporation in wild-type and mutant uteri of 35- to 38-week-old animals. Overall, *Pten*$^{+/-}$ uterine CAH had a 2-fold increase in BrdUrd-positive cells when compared with wild-type secretory epithelium ($+/-$, $n = 4$; wild type, $n = 3$; Fig. 2*A*). Analysis of seven cystic lesions composed of both transformed and untransformed epithelium revealed a 3-fold increase in BrdUrd-positive cells in the transformed epithelium (Fig. 2*B*; $P = 0.007$). At the same time we measured the level of BrdUrd incorporation in the adrenal medulla. We found that there was a substantial increase in the proliferation of medullary cells of *Pten*$^{+/-}$ mice that occurred in regions of neoplasia (Fig. 2 *C–E*; $P < 0.001$).

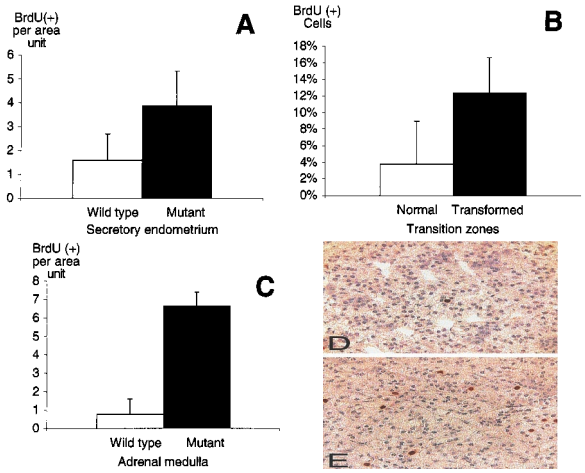

Fig. 2. Increased proliferation in the neoplastic regions of *Pten*$^{+/-}$ uteri and adrenals. Mice were injected with 125 mg/kg of BrdUrd for 1 h before death and sections were stained with an antibody recognizing BrdUrd. (*A*) Proliferation index in *Pten*$^{+/+}$ (□) and *Pten*$^{+/-}$ (■) uteri was calculated by comparing the proliferation index of the secretory epithelium in wild type with that of the CAH. (*B*) Proliferation index in normal (□) and transformed (■) regions of cysts of *Pten*$^{+/-}$ uteri. BrdUrd-positive cells were counted per total number of nuclei. (*C*) Proliferation index of wild-type (□) and $+/-$ (■) adrenal medulla. Error bars indicate SD. Examples BrdUrd staining of the wild-type (*D*) and *Pten*$^{+/-}$ (*E*) medulla. Increased BrdUrd incorporation can be seen in *E* relative to *D*.

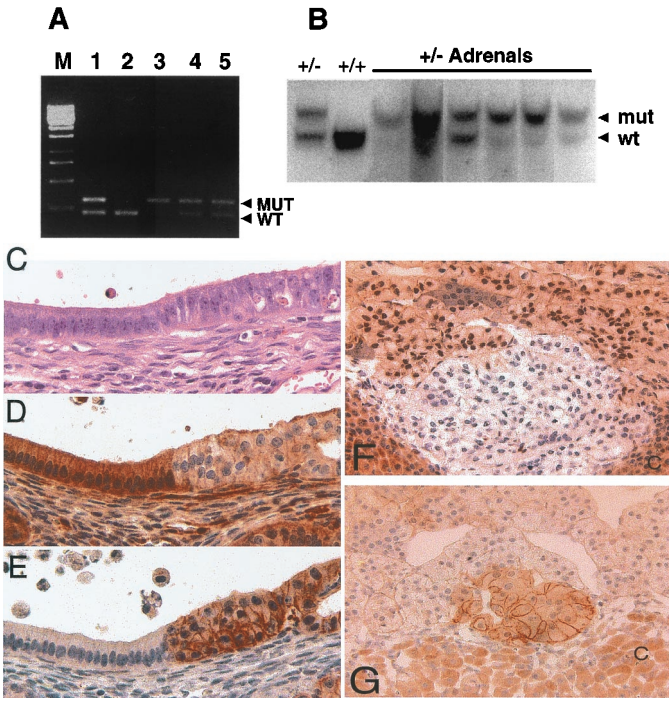

Fig. 3. Neoplastic lesions in *Pten*$^{+/-}$ uteri have lower levels of Pten, and higher active Akt. (*A*) Loss of heterozygosity in hyperplastic lesions of the endometrium. Products from wild-type and mutant *Pten* alleles are amplified in a duplex reaction. Controls consist of products generated from tail DNA isolated from *Pten* heterozygous (lane 1) and wild-type (lane 2) mice. Lanes 3, 4, and 5 are amplified products from microdissected, hyperplastic endometrial lesions from three *Pten* heterozygous mice at 32 weeks of age. Loss of the wild-type *Pten* allele is present in one lesion (lane 3), and both alleles are retained in the other two lesions (lanes 4 and 5). (*B*) Loss of heterozygosity in *Pten*$^{+/-}$ adrenals. Adrenal DNA was prepared from six *Pten*$^{+/-}$ mice. After probing the wild-type (wt) and mutant alleles (mut) (arrowheads), we observed that five of the six *Pten*$^{+/-}$ adrenals had undergone loss of heterozygosity. Control ($+/-$) and wild-type DNA ($+/+$) were prepared from tails. (*C–E*) Transition zone in *Pten*$^{+/-}$-transformed uterine cysts. Slides were stained with hematoxylin/eosin (*C*), rabbit polyclonal anti-PTEN (*D*), and rabbit polyclonal anti-phospho-AKT (Ser-473) (*E*). (Magnification, ×600.) (*F* and *G*) Altered PTEN and phospho-AKT expression are detected in the adrenal medulla. Reduced PTEN staining correlates with transformation and phospho-AKT staining. (*F*) A small representative focus of reduced PTEN expression in a *Pten*$^{+/-}$ adrenal medulla. Notice that most PTEN staining within the medullary cells occurs in the nucleus. (*G*) A small focus of increased phospho-AKT staining correlates with reduced PTEN expression. (Magnification, ×600.) Cortex (C) stains nonspecifically for PTEN and phospho-AKT.

With use of terminal deoxynucleotidyltransferase labeling of DNA nicks with the TUNEL assay on the same tissues, no difference in the apoptotic frequency was observed between wild-type and heterozygous tissues (data not shown).

Loss of the Wild-Type Allele Occurs in the Lesions. Uteri then were examined for loss of wild-type *Pten*. Protein expression analysis of the total lysates of mutant uteri demonstrated reduced PTEN expression relative to wild type (data not shown). PCR analysis of the individual lesions in seven *Pten*$^{+/-}$ mice detected loss of the wild-type *Pten* allele in 30% (9/30) lesions studied (Fig. 3*A*). An example of loss of heterozygosity in a lesion is shown in lane 3; lesions with no discernible loss of heterozygosity are shown in lanes 4 and 5 (Fig. 3*A*). The frequency of loss may be an underestimate because of normal tissue contamination during microdissection. In the adrenal lesions, loss of the wild-type

allele was observed in five of six heterozygous adrenals by Southern blotting (Fig. 3*B*).

Neoplasia Is Characterized by Reduced PTEN Expression and Increased Phosphorylation of AKT. Immunohistochemical analysis of uterine sections demonstrated that untransformed epithelial cells stained intensely for PTEN in the cytoplasm, whereas significantly decreased levels of Pten staining occurred in regions of transformation ($n = 60$; Fig. 3 *C* and *D*). Pten-deficient cells typically have activated AKT. Analysis of phosphorylated Akt in the serial sections of the uteri of *Pten*$^{+/-}$ mice detected phospho-Akt (Ser-473) in all of the areas of transformation ($n = 60$) in a membrane-specific pattern (Fig. 3*E*). The signal also corresponded precisely to the areas of Pten down-regulation. Staining for total AKT revealed that nearly all of the AKT shifted from the cytoplasm and nucleus in normal epithelium to the membrane in CAH (data not shown). We did not detect phospho-Akt in any of the uterine sections of 35- to 38-week-old wild-type mice (data not shown). In the adrenal medulla, staining for PTEN occurred in both the nucleus and cytoplasm of medullary chromaffin cells (Fig. 3*F*). In *Pten*$^{+/-}$ mice, multifocal regions of reduced PTEN expression were found. An example of a focus of reduced staining is shown in Fig. 3*F*. In addition, increased staining for phospho-AKT could be detected in areas of reduced PTEN staining (Fig. 3*G*).

Altered Activity of S6K in the Neoplastic Uterus. Because CAH was consistently found in older *Pten*$^{+/-}$ mice, we decided to determine whether S6K kinase activity was elevated in their uteri. We also tested whether a mTOR inhibitor could affect S6K activity in established endogenous tumors. We chose to use the rapamycin ester, CCI-779, which was developed for i.v. administration in cancer patients (19, ††). For 3 days, 34- to 44-week-old *Pten*$^{+/-}$ females were injected once daily with 20 mg/kg CCI-779 or the vehicle only. The choice of dose was based on prior studies of mouse response to CCI-779 (J.G., unpublished observations). Tissues were collected on the last day of injection from treated ($n = 3$) and untreated ($n = 4$) *Pten*$^{+/-}$ and untreated wild-type ($n = 4$) mice. S6K activity was elevated in the uteri of heterozygous mice relative to wild type (Fig. 4*A*). CCI-779 seemed to inhibit kinase activity to wild-type levels. Uterine lysates also were analyzed for the mobility of S6K, because its slower migrating form is associated with increased phosphorylation and kinase activity. Lysates from starved and epidermal growth factor-pulsed 293 cells were loaded as controls for the detection of the fast- and slow-moving species. The slow-moving species of S6K was observed only in the epidermal growth factor-treated 293 lysate and the lysates from two untreated *Pten* heterozygous uteri (Fig. 4*C*). CCI-779 treatment led to the presence of only the hypophosphorylated, inactive, and faster migrating form. Uteri of *Pten* heterozygous females that received CCI-779 injections for 3 days had a modest 40% reduction in epithelial proliferation (Fig. 4*B*). Although CCI-779 had a marked effect on S6K activity, the level of phospho-Akt (Ser-473) was not affected in either uterine or adrenal tissues (Fig. 4*D*). No difference in apoptosis levels was detected among the different groups as assessed by terminal deoxynucleotidyltransferase labeling of DNA nicks (data not shown).

Trial of CCI-779 in *Pten*$^{+/-}$ Mice. To determine whether CCI-779 could be used to treat the mouse tumors, a longer course of CCI-779 was given. A second group of *Pten*$^{+/-}$ females (24–28 weeks old) were injected daily with 20 mg/kg CCI-779 ($n = 7$) or vehicle ($n = 7$), or were left untreated ($n = 6$) for 10 weeks

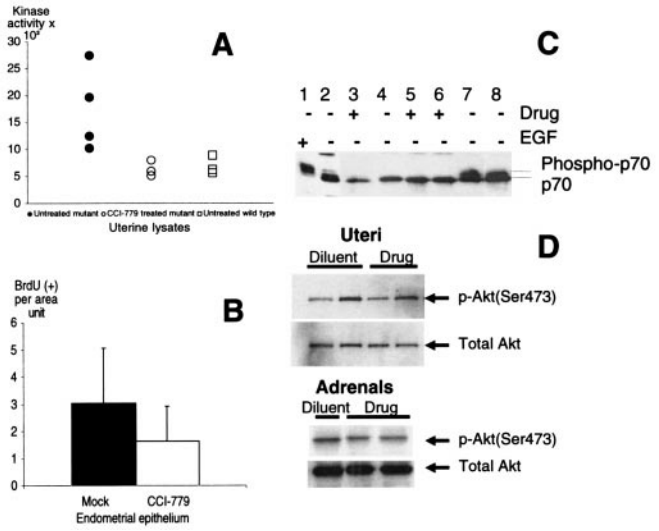

Fig. 4. S6K activity but not AKT phosphorylation can be inhibited with CCI-779. (*A*) S6K activity in *Pten*$^{+/-}$ (●), *Pten*$^{+/-}$ treated with CCI-779 for 3 days (○), and *Pten*$^{+/+}$ (□) uterine lysates. Protein concentration was measured from the soluble fraction, and samples were normalized for equal protein concentration before the immunoprecipitation and measurement of S6K activity. (*B*) Short-term CCI-779 treatment reduces the BrdUrd incorporation index. BrdUrd incorporation index in mock (■)- and drug (□)-treated *Pten*$^{+/-}$ uterine epithelium treated for 3 days with vehicle or CCI-779. (*C*) Phosphorylated S6K levels in 293 cell line and mouse uterine lysates. (Lanes 1 and 2) 293 cells pulsed with epidermal growth factor or starved. Note reduced mobility of S6K in lane 1. *Pten*$^{+/+}$ (lanes 3 and 4) and *Pten*$^{+/-}$ (lanes 5–8) uterine lysates analyzed on an 8% polyacrylamide gel. Frozen uteri were ground and transferred into loading SDS buffer, and protein concentrations were normalized by anti-MAPK signal. A slower migrating band was seen in lysates of mice that were not treated with CCI-779 (lanes 7 and 8). This band was not present in *Pten*$^{+/-}$ lysates of mice treated with CCI-779 for 3 days (lanes 5 and 6) or in treated or untreated wild-type lysates (lanes 3 and 4). (*D*) Uterine (*Upper*) and adrenal (*Lower*) lysates from wild-type (+/+) and mutant animals (+/−) were resolved on a 4–20% gradient gel, blotted, and probed with anti-phospho-473 and total AKT antibodies. Each sample was collected from a *Pten*$^{+/-}$ mouse injected with either diluent or CCI-779 (Drug) for 3 days.

(weeks 1, 2, 4, 6, and 8: 5 days on, 2 days off; weeks 3, 5, 7: 7 days off; week 9: 4 days on, 3 days off; week 10: 2 days on). Tissues were collected on the day after the last injection. Long-term treatment with CCI-779 produced detectable improvement in the health of the animals. Animals receiving drug injections appeared more active, and by the end of the study all were alive, whereas three animals died in the untreated and mock-treated groups. The cause of death was not determined, but was typically caused by uterine or gastrointestinal tumors.

We chose to focus on the drug's effect on the two tumor phenotypes with the highest penetrance by 25 weeks of age, uterine and adrenal medullary neoplasia. Morphological analysis showed that drug-treated *Pten* heterozygotes had a marked reduction in uterine and adrenal lesion size when compared with the mock-treated or untreated group (Fig. 5 *A* and *B*; $P = 0.09$, $P = 0.039$). However, the effect appeared to be cytostatic because lesion size of the treated group and untreated 26-week-old mice was similar. Drug-treated mice also had a substantial reduction in the frequency of BrdUrd incorporation in both types of neoplasia relative to mock-treated controls (Fig. 5 *C* and *D*; $P = 0.028$, $P < 0.001$). Immunohistochemical analysis of uterine sections still detected reduced Pten and activated Akt levels in drug-treated lesions ($n = 35$), indicating that the intervention occurred downstream of these molecules (Fig. 5 *E* and *F*). Although both PTEN and rapamycin have been linked to the regulation of p27, no alteration of p27 was detected by

††Gibbons, J. J., Discafani, C., Petersen, R., Hernandez, R., Skotnicki, J. & Frost, P. (1999) *Proc. Am. Assoc. Cancer Res.* **40,** 301 (abstr.).

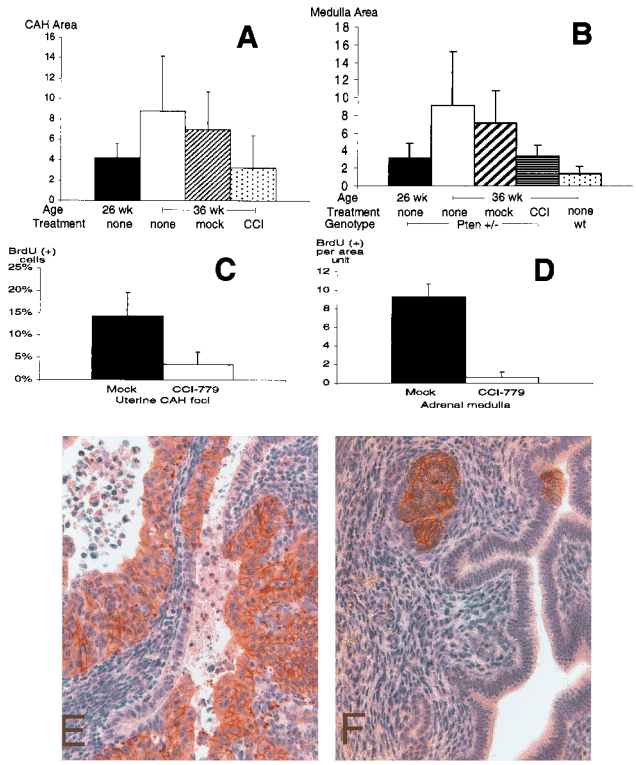

Fig. 5. Long-term CCI-779 treatment prevents tumor growth and proliferation in *Pten*$^{+/-}$ without affecting Akt activity. (*A*) Size of neoplastic lesions in mock, untreated (none) and CCI-779-treated (CCI) uteri. All mice are *Pten*$^{+/-}$ females and average age of each cohort is indicated. (*B*) Size of the untreated (none) wild-type (wt), untreated *Pten*$^{+/-}$, mock-treated *Pten*$^{+/-}$, and CCI-779-treated (CCI) *Pten*$^{+/-}$ adrenal medullas. (*C*) Proliferation in mock (■)- and drug (□)-treated uteri. BrdUrd-positive cells were counted per total number of nuclei in CAH. (*D*) Proliferation in mock-treated *Pten*$^{+/-}$ (■) and CCI-779-treated *Pten*$^{+/-}$ (□) adrenal medullas. (*E* and *F*) Phosoho-473 Akt levels in the mock (*E*)- and drug (*F*)-treated uteri. (Magnification, ×400).

immunohistochemistry in either treated or untreated lesions (40, 41).

Discussion

It is likely that the loss of Pten found in the tumors of *PTEN*$^{+/-}$ mice leads to increased levels of PtdIns(3,4,5)P_3, which in turn is able to activate AKT, 3-phosphoinositide-dependent kinase 1, S6K, mTOR, and many other proteins. In combination, these activated proteins probably contribute to the transformation and increased tumor proliferation that was observed in a variety of organs (Figs. 1 and 2). Of these activated proteins, S6K is likely to play a major role in the progression of the cell cycle into the S phase. Microinjection of anti-S6K antibodies into quiescent rat embryo fibroblasts prevents the mitogenic effect of serum (32, 33). In T cells, which are unable to proliferate in the presence of rapamycin, a rapamycin-resistant allele of S6K is sufficient to rescue the activation of an E2F reporter (42). S6K1$^{-/-}$ mouse embryonic stem cells have an elevated proportion of cells in G_0/G_1 and slower proliferation relative to wild type (10). Finally, dTOR mutation is associated with G_0/G_1 accumulation and lack of animal viability that can be rescued by overexpression of dS6K (32). Such data suggest that inhibition of S6K is an important mediator of the antiproliferative effects of mTOR.

Another regulator of translation and cell growth, 4E-BP1, is controlled by the PI3K/AKT and mTOR pathways (24, 25, 43, 44). In its unphosphorylated state, 4E-BP1 binds to EIF-4E to inhibit the translation of 5′-capped messages (45). On stimulation of cell growth, 4E-BP1 becomes phosphorylated and no longer inhibits translation. Inhibitors of mTOR block phosphorylation of 4E-BP1. Although we have not studied 4E-BP1 phosphorylation, alterations of its function may be contributing to the neoplasias that we see.

We conclude that the tumor stasis and the reduced proliferation that we have observed with the rapamycin analog CCI-779 is in part caused by the inhibition of the elevated S6K activity found in the tumors (Figs. 4 and 5). Our findings suggest that S6K and possibly other proteins regulated by mTOR contribute to the oncogenic effects of Pten loss.

Although we see a reduction in tumor proliferation in the mouse tumors, rapamycin and CCI-779 are not broadly antiproliferative. Rapamycin is well tolerated when administered *in vivo* and inhibits the growth of only a subset of tumors expressing mTOR (46). In a recent report by the Vogt lab, rapamycin was found to inhibit the growth of fibroblasts transformed with AKT and PI3K but had no effect on cells transformed with v-Jun or v-Src (47). This group found that the growth of v-H-Ras and v-Myc transformants was stimulated by rapamycin. It also has been reported that rapamycin is able to induce apoptosis in tumors. We have not seen such apoptosis and presume that this may be a reflection of the benign nature of the mouse neoplasias. Huang *et al*. have recently shed light on this paradox (48). They found that tumor cells and mouse embryo fibroblasts lacking intact p53 or p21 were unable to arrest in G_1 in response to rapamycin and instead underwent apoptosis. However, when the p53 pathway was reconstituted or intact, cells arrested in G_1 and did not die. These data suggest that rapamycin analogs may be more potent in the clinical setting in which the PTEN and p53 pathways are altered.

We have found that disease progression caused by *Pten* mutation can be delayed by inhibiting mTOR and biochemical targets downstream of mTOR such as S6K. This finding suggests that enzymes other than AKT are excellent targets for the treatment of *PTEN*$^{-/-}$ tumors. With respect to human endometrial cancers, which lack PTEN in more than 60% of cases, inhibition of mTOR may prove to be a useful agent for patients with disease that is refractory to standard treatments. Moreover, rapamycin and its analog CCI-779 are well tolerated in people, suggesting that there may be a usable therapeutic dose with limited systemic toxicity (19). In the future, it will be interesting to determine in *Pten*$^{+/-}$ mice whether the inducible disruption of *S6K1*, *mTOR*, or *4E-BP1* or a combination of these will have antitumor effects that are similar to CCI-779.

We thank Giorgio Cattoretti for his assistance with immunohistochemical staining and generous sharing of reagents. R.T.L. was supported by the Peter Jay Sharp Foundation, the Don Shula Foundation, and the American Society of Clinical Oncology. This work was supported by National Cancer Institute Grant CA 75553.

1. Ali, I. U., Schriml, L. M. & Dean, M. (1999) *J. Natl. Cancer Inst.* **91,** 1922–1932.
2. Cantley, L. C. & Neel, B. G. (1999) *Proc. Natl. Acad. Sci. USA* **96,** 4240–4245.
3. Stambolic, V., Suzuki, A., de la Pompa, J. L., Brothers, G. M., Mirtsos, C., Sasaki, T., Ruland, J., Penninger, J. M., Siderovski, D. P. & Mak, T. W. (1998) *Cell* **95,** 29–39.
4. Sun, H., Lesche, R., Li, D. M., Liliental, J., Zhang, H., Gao, J., Gavrilova, N., Mueller, B., Liu, X. & Wu, H. (1999) *Proc. Natl. Acad. Sci. USA* **96,** 6199–6204.
5. Huang, H., Potter, C. J., Tao, W., Li, D. M., Brogiolo, W., Hafen, E., Sun, H. & Xu, T. (1999) *Development (Cambridge, U.K.)* **126,** 5365–5372.
6. Goberdhan, D. C., Paricio, N., Goodman, E. C., Mlodzik, M. & Wilson, C. (1999) *Genes Dev.* **13,** 3244–3258.
7. Gao, X., Neufeld, T. P. & Pan, D. (2000) *Dev. Biol.* **221,** 404–418.
8. Montagne, J., Stewart, M. J., Stocker, H., Hafen, E., Kozma, S. C. & Thomas, G. (1999) *Science* **285,** 2126–2129.
9. Leevers, S. J. (1999) *Science* **285,** 2082–2083.

DOCKET ALARM

Explore Litigation Insights

Docket Alarm provides insights to develop a more informed litigation strategy and the peace of mind of knowing you're on top of things.

Real-Time Litigation Alerts

Keep your litigation team up-to-date with **real-time alerts** and advanced team management tools built for the enterprise, all while greatly reducing PACER spend.

Our comprehensive service means we can handle Federal, State, and Administrative courts across the country.

Advanced Docket Research

With over 230 million records, Docket Alarm's cloud-native docket research platform finds what other services can't. Coverage includes Federal, State, plus PTAB, TTAB, ITC and NLRB decisions, all in one place.

Identify arguments that have been successful in the past with full text, pinpoint searching. Link to case law cited within any court document via Fastcase.

Analytics At Your Fingertips

Learn what happened the last time a particular judge, opposing counsel or company faced cases similar to yours.

Advanced out-of-the-box PTAB and TTAB analytics are always at your fingertips.

API

Docket Alarm offers a powerful API (application programming interface) to developers that want to integrate case filings into their apps.

LAW FIRMS
Build custom dashboards for your attorneys and clients with live data direct from the court.

Automate many repetitive legal tasks like conflict checks, document management, and marketing.

FINANCIAL INSTITUTIONS
Litigation and bankruptcy checks for companies and debtors.

E-DISCOVERY AND LEGAL VENDORS
Sync your system to PACER to automate legal marketing.